Analysis and Experimental Validation of Control Systems for Four-Leg Matrix Converter Applications

Roberto Cárdenas, *Senior Member, IEEE*, Carlos Juri, *Student Member, IEEE*, Rubén Peña, *Member, IEEE*, Jon Clare, *Senior Member, IEEE*, and Patrick Wheeler, *Member, IEEE*

***Abstract*—Matrix Converters (MCs) have some advantages when compared to conventional back-to-back PWM voltage source converters. The converter may be considered more reliable and it can be smaller because the bulky dc capacitors are eliminated from the topology. For ac to ac power conversion, the size and weight of the whole generation system can be much reduced when back-to-back converters are replaced by MCs. To supply electrical energy to an unbalanced 3Φ stand-alone load, a fourth leg is required to provide a path for the zero-sequence load current. To regulate the load voltage, closed-loop control is required. In this paper, the application of *d–q* controllers and resonant controllers to four-leg MCs is addressed. The design and performance issues of the controllers, for operation with balanced, highly unbalanced loads and nonlinear loads are discussed in this paper. Experimental results obtained from a small prototype are presented and analysed in detail.**

***Index Terms*—AC–AC power conversion, control system, power generation.**

I. Introduction

MATRIX CONVERTERS (MCs) have many advantages, which are well documented in the literature [1]–[5]. The MC provides bi-directional power flow, sinusoidal input/output currents and controllable input displacement factor [1], [4], [6]. When compared to back-to-back converters, the MC has some significant advantages. For instance, due to the absence of electrolytic capacitors, the MC can be more robust and reliable [2]. The space saved by a MC compared to a conventional back-to-back converter has been estimated as a factor of three [3].

MCs can be used in portable generation systems, for instance in those employing variable speed diesel engines [5], [7]. However, in this case a four-leg MC is required, to provide a path for the zero-sequence currents. The topology of the four-leg MC system considered in this work is shown in Fig. 1. A second-order LC filter is used at the MC input to improve the quality of the input currents [8], [9]. The input filter capacitors also provide the essential decoupling to minimize the commutation inductance between phases. Usually a resistor in parallel with the input inductance (see Fig. 1) improves the damping of the system [10], [11]. At the MC output a second-order LC filter is provided to reduce the amplitude of the switching harmonics in the load voltages [6], [7], [12]. Fig. 1 also shows the star-connected stand-alone load that the four-leg MC is assumed to feed.

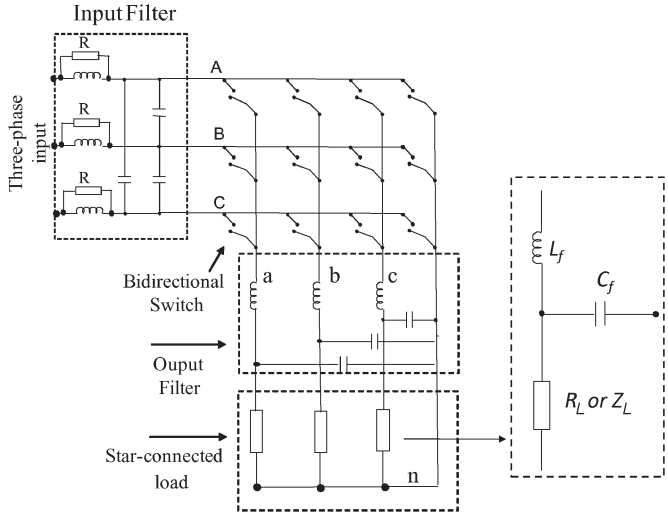

Fig. 1. Matrix converter and input/output filters.

Control systems and modulation algorithms for four-leg matrix converters have recently been reported in the literature [9], [12], [13]. A space vector modulation (SVM) algorithm was recently presented in [9], [14], a standard d–q voltage control system was reported in [5] and resonant controllers have been discussed in [13].

The performance of the d–q control system reported in [5] is appropriate when the system is operating with slightly unbalanced linear load or when the total impedance between the four-leg MC output and the load is small. Otherwise a control system implemented in a synchronous rotating frame cannot eliminate the negative and zero-sequence components from the load voltages. Sequence components of unbalanced 3ϕ systems are discussed in more detail in [15]–[18].

As an alternative to d–q controllers, systems employing resonant controllers can be applied to four-leg power converters [13]. Moreover, the distortion produced by nonlinear loads can be eliminated using several RCs in a cascade implementation [19]. However, the methodology reported in the literature for designing resonant controllers is not always appropriate for the control of high-order plants. For instance, one of the methods

Manuscript received October 28, 2010; revised February 18, 2011, April 18, 2011, and May 7, 2011; accepted May 9, 2011. Date of publication May 27, 2011; date of current version October 4, 2011. This work was supported by Fondecyt Chile under Contract 1110984.

R. Cárdenas and C. Juri are with the Electrical Engineering Department, University of Chile, 8370451 Santiago, Chile (e-mail: rcd@ieee.org; carlos.juri@gmail.com).

R. Peña is with the Electrical Engineering Department, University of Concepción, 4074580 Concepción, Chile (e-mail: rupena@udec.cl).

J. Clare and P. Wheeler are with the Department of Electrical and Electronic Engineering, University of Nottingham, Nottingham NG7 2RD, U.K. (e-mail: jon.clare@nottingham.ac.uk; pat.wheeler@nottingham.ac.uk;).

Color versions of one or more of the figures in this paper are available online at http://ieeexplore.ieee.org.

Digital Object Identifier 10.1109/TIE.2011.2158041

reported previously is to use resonant controllers with the same proportional and integral gains of PI controllers designed in a synchronous rotating frame [20]–[23]. However, this is hardly appropriate for the application depicted in Fig. 1, because a single PI controller is not sufficient to ensure good dynamic performance in the whole operating range when a second or higher-order load is fed by the MC. Other design methods have been reported, for instance in [22] it is proposed, without much analysis, to use a low-pass to high-pass transformation to referrer a controller designed in the synchronous frame to the stationary frame.

Because of the lack of appropriate design methods for resonant controllers aimed to regulate the voltage of stand-alone unbalanced loads, design methodologies are discussed in this work. In Section II of this paper, the equivalence between resonant controllers implemented in the a–b–c frame and controllers designed in synchronous rotating frames are discussed. The use of the frequency shifting property of the Laplace transform is used to analyse the frequency response of the control systems [24]–[26]. In this section it is analytically shown that some of the conventional methods used to refer d–q controllers to the stationary frame do not produce resonant controllers with an exact equivalence in terms of bandwidth and dynamic performance.

In Sections II-B and III the implementation of digital resonant controllers applied to four-leg matrix converters is discussed. Two design approaches are presented and discussed. In Sections IV and V, the experimental results are presented and discussed. In Section IV it is shown that a conventional d–q control system implemented in a positive sequence synchronous rotating frame can also be applied to regulate the voltage of unbalanced linear/nonlinear loads fed by a four-leg matrix converter when the output filter inductance is relatively small. Finally, an appraisal of the proposed control methods is presented in the Conclusion.

For all the experimental work the SVM algorithm reported in [9] is used. The design and implementation of SVM algorithms for four-leg MCs is considered outside the scope of this paper and the interested reader is referred elsewhere [9], [14].

II. Control Systems Approaches for Four-Leg Matrix Converters

A. Conventional d–q Control Systems

Control systems based on synchronously rotating reference frames are a standard method for the regulation of voltages and currents in electrical machines and power converters [27]–[29]. Using d–q rotating frames, 3ϕ voltages and currents are transformed into dc signals for steady state operation.

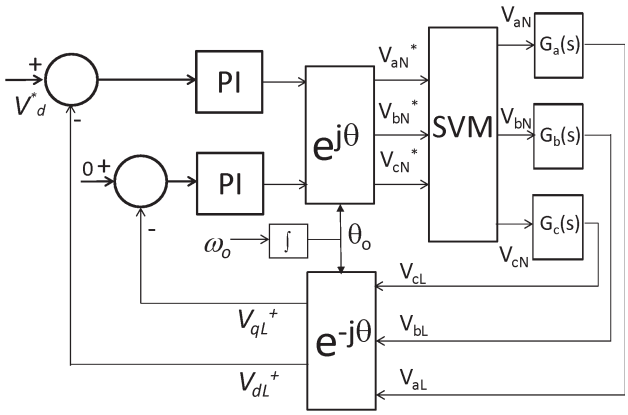

Fig. 2. Control diagram for a standard d–q control system for a four-leg matrix converter.

The d–q control topology proposed for four-leg MCs is shown in Fig. 2. The block labeled SVM includes the modulation algorithm and the converter. The load voltages are referred to a d–q frame rotating at the output frequency ω_o. The transfer functions $G_a(s)$, $G_b(s)$ and $G_c(s)$ relate the line to neutral four-leg MC output voltage with the corresponding load voltage. In a–b–c coordinates, the transfer function between the phase to neutral voltages and the load voltages is (see Fig. 1)

$$G_a(s) = \frac{V_{aL}}{VaN} = \frac{R_{La}}{s^2 R_{La} C_f L_f + s L_f + R_{La}} \tag{1}$$

where V_{aN} is the line to neutral voltage of phase "a" at the MC output; R_{La} is the resistive load in phase a; L_f and C_f are the parameters of the second-order power filter (see Fig. 1) and "s" is the Laplace operator. The transfer functions $G_b(s)$ and $G_c(s)$ are obtained by replacing R_{La} with R_{Lb} and R_{Lc}, respectively.

To design the system in a synchronous rotating frame, the plant dynamics in α–β coordinates have to be transferred to d–q coordinates. In this paper, the frequency shifting property of the Laplace transform is used for this analysis, instead of the rather complex time domain approach presented previously in [22], [30]. The frequency shifting property of the Laplace transform is represented by

$$\mathcal{L}\left(f(t)e^{-j\omega_o t}\right) = F(s + j\omega_o) \tag{2}$$

where the symbol "$\mathcal{L}$" represents the Laplace transform. In this paper, to refer a transfer function from the stationary frame (positive sequence) α–β to d–q, the operator "s" is replaced by "$s + j\omega_o$". On the other hand, to refer a transfer function from d–q to α–β, the operator "s" is replaced by "$s - j\omega_o$". Therefore, the transfer function of (1) can be referred to the synchronous rotating frame as (3), shown at the bottom of the page.

$$\begin{aligned} G_{dq}(s) = \frac{\overline{V}_{dqL}}{\overline{V}_{dqN}} &= \frac{R_{La}}{(s + j\omega_o)^2 R_{La} C_f L_f + (s + j\omega_o) L_f + R_{La}} \\ &= \frac{R_{La}}{s^2 C_f L_f R_{La} + (L_f + 2jL_f C_f R_{La}\omega_o)s + (j\omega_o L_f + R_{La} - C_f L_f R_{La}\omega_o^2)} \end{aligned} \tag{3}$$

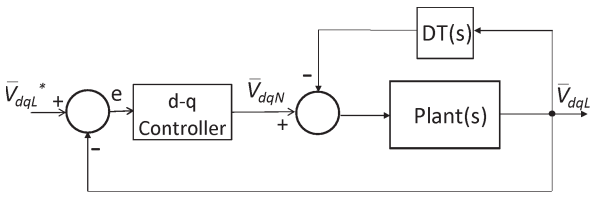

Fig. 3. Simplified d–q control system considering decoupling terms.

Using (3) the voltage at the controller output is related to the load voltage as

$$\begin{bmatrix} V_{dN} \\ V_{qN} \end{bmatrix} = A(s) \begin{bmatrix} V_{dL} \\ V_{qL} \end{bmatrix} \tag{4}$$

with the matrix A(s) defined as (5), shown at the bottom of the page. The terms relating the d-axis controller output with the q-axis load voltage (and vice versa) are called "cross-coupling" terms which are usually introduced by the presence of the complex operator "j" in the transfer function of the plant or controller. In d–q control systems, it is a standard practice to add decoupling terms to the controller output to eliminate the cross-coupling [31], [32]. This is shown in Fig. 3, where the label "DT" stands for "Decoupling Terms".

The decoupling terms are plant dependent. For the plant of (3), it can be shown that these terms are

$$\begin{aligned} \frac{Plant(s)}{1 + DT(s)Plant(s)} &= \frac{R_{La}}{s^2 R_{La} C_f L_f + s L_f + R_{La}} \rightarrow DT(s) \\ &= (2jC_f L_f \omega_o s + jL_f \omega_o / R_{La} \\ &\quad - C_f L_f \omega_o^2) \, \overline{V}_{dqL}(s) \end{aligned} \tag{6}$$

where $Plant(s)$ is the transfer function of (3).

Because of the difficulties associated with the implementation of a real time differentiation, $DT(s)$ can be approximated to

$$DT(s) \approx \left(jL_f \omega_o / R_a - C_f L_f \omega_o^2 \right) \overline{V}_{dqL}(s). \tag{7}$$

After some manipulation it is relatively simple to demonstrate that (7) can be simplified to

$$DT(s) \approx j\omega_o L_f \bar{i}_{dq}(s) \tag{8}$$

where $\bar{i}_{dq}$ is the MC output current vector. In a matrix converter this current is usually measured, because it is required in the modulation algorithm [8].

The frequency response of the closed-loop transfer function $\overline{V}_{dqL}(s)/\overline{V}^{*}_{dqL}(s)$ (see Fig. 3) is shown in Fig. 4. Negative frequencies are shown in this graphic to facilitate comparing the frequency response of Fig. 4, with the corresponding closed-loop frequency response obtained with RCs in Section II-B.

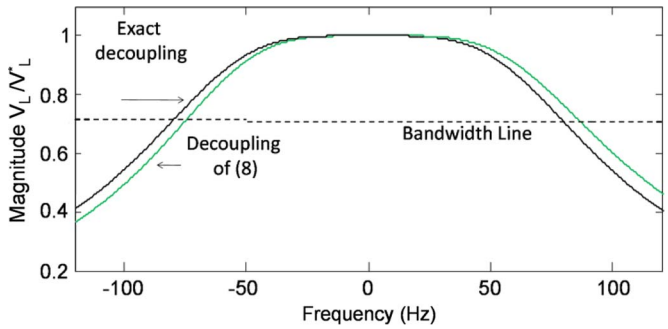

Fig. 4. Bode plot of the transfer function $\overline{V}_{dqL}(s)/\overline{V}^{*}_{dq}(s)$ (see Fig. 3), considering exact decoupling and the decoupling of (8).

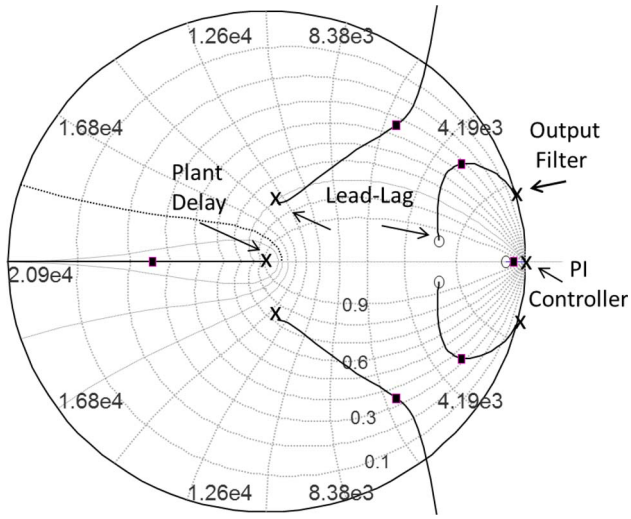

Fig. 5. Root-Locus of the d–q control system.

For the results shown in Fig. 4 the d–q controllers have been designed for a Phase Margin (PM) of 65° and a bandwidth of about 80 Hz. For the plant the values of $R_L = 10\ \Omega$, $C_f = 40\ \mu$F and $L_f = 5$ mH have been considered. As shown in Fig. 4, only a small bandwidth variation is produced when the simplified decoupling of (8) is used.

Controllers implemented in synchronous rotating axis have advantages and disadvantages when applied to four-leg matrix converters. The design is simple and the "s" domain plant does not change with the output frequency when decoupling terms are considered. The best performance with d–q controllers is achieved when the load is balanced, slightly unbalanced, and/or when the filter inductance in the second-order output filter is very small, i.e., $G_a(s)$, $G_b(s)$, and $G_c(s) \approx 1$ [see (1)]. However, because of the small inductance, the switching frequency has to be relatively high to reduce the load total harmonic distortion (THD). Therefore, a rather fast digital signal processing (DSP) platform has to be used to implement the modulation and control algorithm.

$$A(s) = \begin{bmatrix} \left(C_f L_f s^2 + \frac{L_f}{R_{La}} s + \left(1 - C_f L_f \omega_o^2\right) \right) & -\left(2C_f L_f \omega_o s + \frac{L_f}{R_{La}} \omega_o \right) \\ \left(2C_f L_f \omega_o s + \frac{L_f}{R_{La}} \omega_o \right) & \left(C_f L_f s^2 + \frac{L_f}{R_{La}} s + \left(1 - C_f L_f \omega_o^2\right) \right) \end{bmatrix} \tag{5}$$

Assuming the plant described by (1), the z-plane root locus for the design of a d–q voltage control system is shown in Fig. 5. A time delay of one sample period is added to the plant to represent the digital implementation of the modulation algorithm. The control loops are designed to have appropriate dynamic response in the worst case situation, i.e., without any load connected to the output ($R_{\mathrm{La}} \rightarrow \infty$ in (1)). Because a single PI controller is not sufficient to provide good dynamic response in the whole operating range, a second-order lead-lag network is added to the controller (see Fig. 5).

B. Resonant Control Systems

A control system implemented in d–q coordinates can be referred to the stationary α–β axis using the frequency shifting property of the Laplace transform. Therefore, a PI controller in the d–q axis is transformed to

$$\left[\frac{k_p(s+a)}{s}\right]_{dq} \overset{dq2\alpha\beta}{\Longrightarrow} \left[\frac{k_p\left((s-j\omega_o)+a\right)}{s-j\omega_o}\right]_{\alpha\beta}. \tag{9}$$

After some manipulation it is relatively simple to demonstrate that the PI controller in a d–q axis is equivalent to a resonant controller in the α–β axis. This is written as

$$\left[\frac{k_p(s+a)}{s}\right]_{dq} \overset{dq2\alpha\beta}{\Longrightarrow} \left[\frac{k_p\left(s^2+as+\left(\omega_o^2+aj\omega_o\right)\right)}{s^2+\omega_o^2}\right]_{\alpha\beta}. \tag{10}$$

Therefore, using the frequency shifting property of the Laplace transform, equivalent controllers can be implemented in either the d–q or α–β frames. The α–β controller of (10) has high gains for error signals with frequency close to ω_{o}. These controllers are usually called Resonant Controllers (RCs)

Using the frequency shifting property of (2), the decoupling terms of (10) can also be transformed to α–β coordinates as

$$DT_{\alpha\beta}(s) = jL_f\omega_o\bar{i}_{\alpha\beta}(s). \tag{11}$$

In most of the reported cases, and even for three-leg inverters feeding balanced loads, the decoupling terms are not considered when a resonant controller is implemented. To the best of our knowledge only one recent publication discusses the use of decoupling terms in resonant controllers [25] concluding that including this term improves the bandwidth of the closed-loop system [this is also shown in Fig. 8(a) and (b)].

Even when the controllers of (9) and (10) are equivalent in terms of bandwidth and PM, the RC of (10) has cross-coupling terms between the α–β components. This is not appropriate for four-leg matrix converters feeding highly unbalanced loads, because the zero-sequence components of the load voltage are not eliminated unless three independent RCs are used to regulate each phase to neutral load voltage. This topology is shown in Fig. 6, and a simplified single block diagram of Fig. 6 is shown in Fig. 7.

There is no reported methodology to implement a resonant controller in a–b–c coordinates (i.e., without the presence of the complex "j" operator in the RC transfer function) with a bandwidth and PM completely equivalent to a corresponding

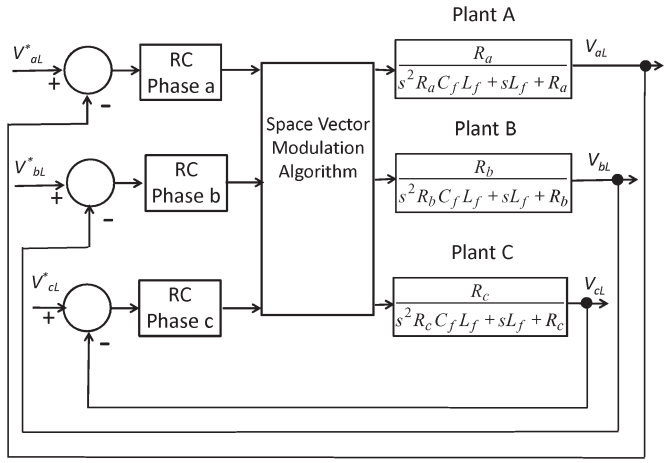

Fig. 6. Resonant controllers, SVM algorithm, and plants.

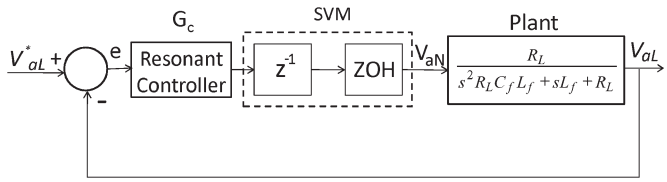

Fig. 7. Simplified single-phase equivalent of Fig. 6.

d–q positive sequence controller. For instance in [21], [22] it is proposed to transform a d–q controller to the α–β frame using the following approximations:

$$[G_c(s)]_{\alpha\beta} \rightarrow \frac{1}{2}\left[G_c(s+j\omega_o)+G_c(s-j\omega_o)\right]_{dq} \tag{12}$$

or using [20]

$$[G_c(s)]_{\alpha\beta} \rightarrow \left[G_c(s+j\omega_o)+G_c(s-j\omega_o)\right]_{dq}. \tag{13}$$

These transformations produce controllers without cross-couplings. However, the dynamic responses of $[G_{\mathrm{c}}(s)]_{\alpha\beta}$ are not equal to that of $[G_{\mathrm{c}}(s)]_{\mathrm{dq}}$. To study the performance of the controllers obtained from (10), (12) and (13), the d–q controller corresponding to the Bode diagram of Fig. 4 has been transformed into resonant controllers using (10), (12) and (13).

The corresponding closed-loop frequency responses are shown in Fig. 8. Fig. 8(a) shows the response considering the RC obtained from (10) with the cross coupling term of (11) considered. Figs. 8(a) and 4 are identical with one of the magnitudes shifted by 50 Hz to the right. In this case the RC is completely equivalent to the d–q controller.

Fig. 8(b), shows the closed-loop frequency response obtained from (12). The bandwidth is reduced [when compared to that obtained in Fig. 8(a)]. Moreover, because the cross-coupling is eliminated, the s-domain plant is no longer constant and the phase margin is dependent on the output frequency. For instance the PM for an output frequency of 25 Hz is $\approx 65^\circ$. However, for an output frequency of 120 Hz, the PM reduces to about 50°.

Fig. 8(c) shows the closed-loop frequency response obtained when the resonant controller is obtained using (13). In this case the PM for $\omega_{\mathrm{o}} = 25$ Hz is about 50° and PM $= 40^\circ$ when the output frequency is 120 Hz. From the viewpoint of the dynamic response, this is the controller with the worst performance.

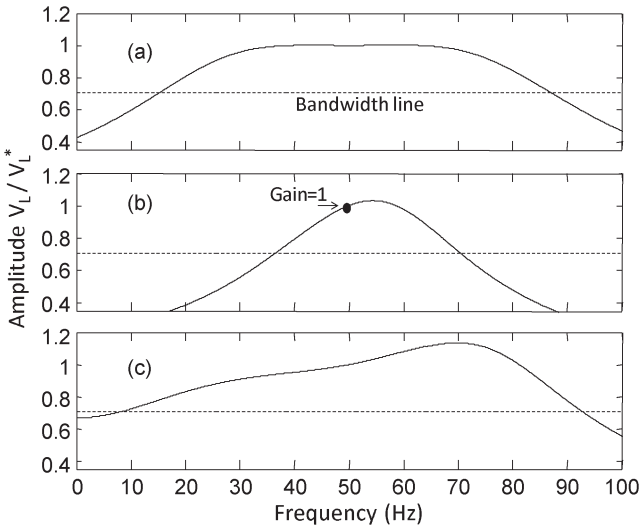

Fig. 8. Bode plots for resonant controllers. (a) Resonant controller of (10) including decoupling terms. (b) Resonant controller of (12). (c) Resonant controller of (13).

Therefore, neither (12) nor (13) are able to fully maintain the dynamic response of a d–q controller designed for regulating a positive sequence signal. This results is in broad agreement with the research reported in [25], [34] where three resonant controllers, derived from a single d–q control system are compared using simulation. It is demonstrated in [34] that when the decoupling terms of DT(s) and the cross-coupling terms of (10) are neglected, the settling time obtained with the resonant controller is larger with relatively poor damped oscillations in the time response. Moreover, in [25] is shown that the frequency response obtained with a resonant controller derived from (12) is much more sensitive to changes in the reference output frequency than the original d–q controller [the same conclusion is obtained by comparing Fig. 8(a) and (b)].

It has been reported in [20], [33] that (13) is equivalent to the transformed PI controllers designed in the positive and negative synchronous rotating frames, to the stationary frame. However, this is not completely correct from the implementation viewpoint. Most of the control systems designed to regulate positive and negative sequence signals, require a notch filter, tuned to twice the operating frequency, to decouple the positive/negative sequence control systems [32]. These filters are not usually considered in the reported implementation of (13). The dynamic effects of the notch filters are not negligible and they cannot be ignored if equivalent controllers between the d–q and stationary frame are required.

Because the reported control methods used to design resonant controllers are not always appropriate, especially when high-order plants are considered, in this work linear control design methods, as Bode and root-locus are applied to the design.

III. Digital Implementation of Resonant Controllers

As stated in the previous section, for the application studied in this work the preferred implementation of RCs is in a, b, c coordinates, regulating the output voltage of each phase

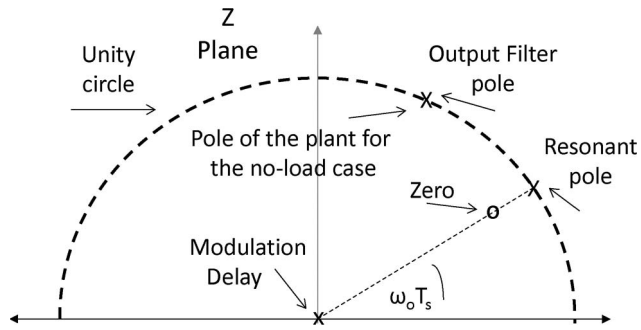

Fig. 9. Poles and zeros of the resonant controller and output filter.

with respect to the neutral connection "n". Without considering cross-couplings, the RC is composed of a couple of purely imaginary poles with a resonant frequency of ω_o, where ω_o is the desired output frequency [33]

$$G_c(s) = K_c \frac{s^2 + 2\zeta\omega_n s + \omega_n^2}{s^2 + \omega_o^2} \tag{14}$$

K_c is the controller gain. In the z-plane, the transfer function of the resonant controller is [19], [35]

$$G_c(z) = K_c \frac{z^2 + a_1 z + a_2}{z^2 + b_1 z + b_2}. \tag{15}$$

In this case the resonant poles are located along the unit circle, as shown in Fig. 9, with an angle with respect to the real axis of $\omega_o T_s$ rads, where T_s is the sampling time and ω_o is the output frequency.

In the frequency domain, the tracking error $e(j\omega_o)$ is calculated as (see Fig. 6)

$$e(j\omega_o) = \frac{V_{aL}^*(j\omega_o)}{1 + G_c(j\omega_o) SVM(j\omega_o) Plant(j\omega_o)}. \tag{16}$$

The operating principle of the RC is that $|G_c(j\omega)| \to \infty$ for a frequency $\omega = \omega_o$ [see (14)]. Therefore, the error calculated from (16) is zero for a sinusoidal reference voltage (V_{aL}^*) of frequency ω_o. However, in a practical implementation the numerical resolution of the DSP platform as well as the interaction between the poles and zeros located at different frequencies, reduces the gain $|G_c(j\omega_o)|$ [35], [36]. This is shown in Fig. 10. Nevertheless, according to the experimental results shown in the next section, the controller gains obtained in the experimental rig are appropriate for the regulation of heavily unbalanced and/or nonlinear loads.

A. Implementing a Resonant Controller From a d–q Design

A first approximation of a digital RC could be obtained from a controller using the frequency shifting property of the Laplace transform [see (2)]. In the z-domain

$$z = e^{sT_s} \tag{17}$$

where T_s is the sampling frequency. In the continuous domain to replace "s" by "$s - j\omega_o$" is equivalent to replace "z" by "$ze^{-\mathrm{j}\omega_o T s}$" in the discrete domain. Therefore, from (12), in a,

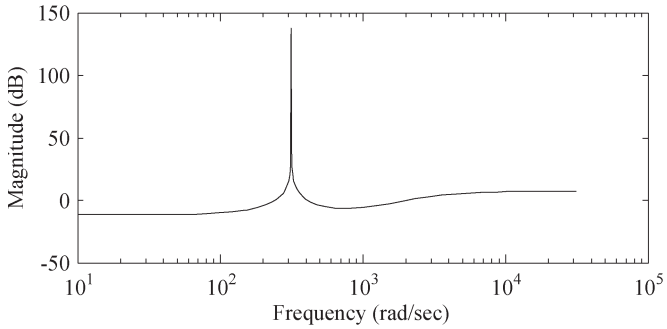

Fig. 10. Bode diagram of the RC magnitude for a practical implementation.

b, c coordinates a first approximation of a digital RC can be obtained from a d–q controller using the expression

$$[G_c(z)]_{\alpha\beta} \rightarrow \frac{1}{2}\left[G_c(ze^{j\omega_o T_s}) + G_c(ze^{-j\omega_o T_s})\right]_{dq} \quad (18)$$

which is the z-domain equivalent of (12). Using (18), a RC is derived from a PI controller implemented in the d–q frame as

$$\left[k_p \frac{z-a}{z-1}\right]_{dq} \xrightarrow{(18)} \left[\frac{k_p\left(z^2-(1+a)\cos(\omega_o T_s)z+a\right)}{z^2-2\cos(\omega_o T_s)z+1}\right]_{\alpha\beta}. \quad (19)$$

An initial design of a resonant controller in the z-domain can be obtained from (18) and (19). However, it has be considered that neither (12) nor (18) maintains the dynamic characteristics of the original controller. Therefore, reshaping of the frequency response using Bode diagrams or Root-locus has to be used to correct the response of the resonant controller in the bandwidth of interest.

B. Design of a Resonant Controller Using Standard Control Design Methods

Some standard design methodologies, such as root locus or Bode plots [37], can be used to design digital resonant controllers in the z-plane. In fact this approach has some advantages because it is simpler to include other effects, e.g., plant and serial A/D converter delays, when standard design tools are applied. In this paper,z-domain root-locus are used to design d–q controllers as well as RCs.

As mentioned before, the controllers should have appropriate dynamic response in the worst case situation, i.e., with no load connected to the output. Therefore, in this case the damping coefficient of the output stage is close to zero and the plant is composed only of the complex poles of the second-order output filter. To improve the dynamic performance of the control system, a second-order lead-lag network is used.

The root locus of the plant + RC is shown in Fig. 11. The plant parameters depicted in the Appendix are used to obtain Fig. 11 The resonant controller poles/zeros are located in the dashed box at the right of the root locus. A zoomed view of the resonant controller poles/zeros is shown below the z-plane unit circle.

In this paper, the RC and associated lead-lag network have been designed to obtain damping ratios above ≈0.3 for all the

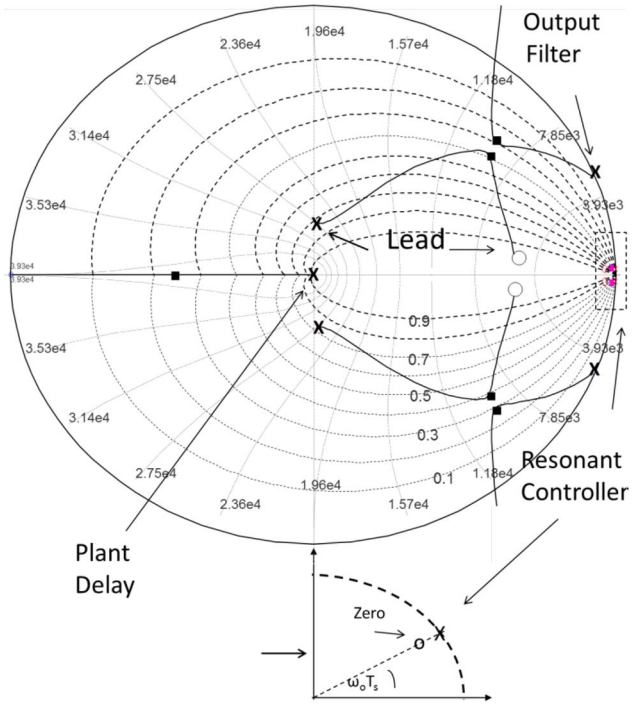

Fig. 11. Design of the closed-loop RC using root locus in the z-plane.

closed-loop poles. For the control system implemented in the experimental rig discussed in Section IV, with $L_f = 5$ mH, $C_f = 40$ μF, $T_s \approx 100$ μS and $\omega_o = 50$ Hz, a suitable RC which meets this design criteria is

$$G_c(s) = 4.9\frac{(z^2-1.926z+0.9276)}{(z^2-1.99z+1)}\frac{(z^2-1.336z+0.45)}{(z^2-0.024z+0.042)} \quad (20)$$

where the first term after the gain is the RC and the last term is the lead-lag network. A closed-loop bandwidth of about 60 Hz is obtained with this voltage controller.

C. Design of a Resonant Control System to Eliminate Harmonic Distortion

When nonlinear loads are connected to the four-leg MC output, a resonant control system can be also used to eliminate most of the harmonic distortion from the load voltages [27].

This is achieved by locating a pair of poles and zeroes in the z-plane to eliminate the most important harmonics contributing to the THD of the load voltage. A cascaded controller is obtained as

$$G_c(s) = K_c\left(\frac{s^2+2\zeta\omega_n s+\omega_n^2}{s^2+\omega_o^2}\right)\left(\frac{s^2+2\zeta\omega_{na}s+\omega_{na}^2}{s^2+\omega_{oa}^2}\right) \times \left(\frac{s^2+2\zeta\omega_{nb}s+\omega_{nb}^2}{s^2+\omega_{ob}^2}\right)\left(\frac{s^2+2\zeta\omega_{nm}s+\omega_{nm}^2}{s^2+\omega_{om}^2}\right) \quad (21)$$

where the poles of each transfer function are tuned to track a particular frequency. In (21) the subscripts "$a, b \ldots m$" are used to indicate harmonics of order a, b, m etc.

With the controller of (21), $|G_c(j\omega)| \rightarrow \infty$ for the frequencies $\omega = \omega_o, \omega = a\omega_o, \omega = b\omega_o, \ldots \omega = m\omega_o$. Therefore, the

tracking error is theoretically zero for all those frequencies [see (16)]. For instance the z-domain transfer function of a controller designed to track a 50-Hz reference signal, eliminating the dc, second, third, fourth, and fifth harmonic is

$$G_c(z) = 2 \cdot \left(\frac{z-0.9872}{z-1}\right) \cdot \left(\frac{z^2-1.942z+0.9462}{z^2-1.996z+1}\right) \cdot \left(\frac{z^2-1.954z-0.9681}{z^2-1.984z+1}\right) \cdot \left(\frac{z^2-1.86z+0.8832}{z^2-1.965z+1}\right) \cdot \left(\frac{z^2-1.938z+0.9743}{z^2-1.937z+1}\right) \cdot \left(\frac{z^2-1.906z+0.9741}{z^2-1.902z+1}\right) \cdot \left(\frac{z^2-1.863z+0.9508}{z^2-1.295z+0.6889}\right). \quad (22)$$

The 13th-order transfer function of (23) is implemented using a state space digital implementation in the DSP platform. All the matrices required are sent from the controller design software to the DSP board. Because of the high complexity in implementing the 13th-order RC discussed above, the sampling time had to be increased to 200 μS.

IV. Experimental Results Obtained With a d–q Controller

The control methodology discussed in this work has been validated using the experimental system shown in Fig. 12. The SVM algorithm and proposed control systems are implemented using a DSP-based control board and an FPGA, the latter implementing the four-step commutation method [1] and generating the switching signals for the IGBT gate drivers. The MC is connected to a three-phase variable transformer at the input. At the output the MC is connected to a three-phase load via a second-order LC output filter to reduce the harmonic content in the voltages and currents. For data acquisition an external board, with 10 analog-to-digital (ADC) channels of 14 bits, 1 μs conversion time each is interfaced to the DSP. This board also has four digital-to-analog (DAC) channels available, which are used to fire a solid state relay to produce load step variations. Hall-effect transducers are used to measure the input currents, input voltages and output currents. Anti-aliasing filters are applied to the measurements. A digital storage oscilloscope is used to measure steady state signals from the experimental system. A host parallel interface (HPI) is use to connect the DSP board to the host computer through a standard USB interface.

Unless otherwise stated, the sampling time used by the SVM and control algorithm is 100 μs.

As mentioned before, the d–q controller presented in this work has good performance when the L_f impedance (see Fig. 12) is small. In this case a d–q controller can be used to adequately regulate the output voltage of a four-leg MC.

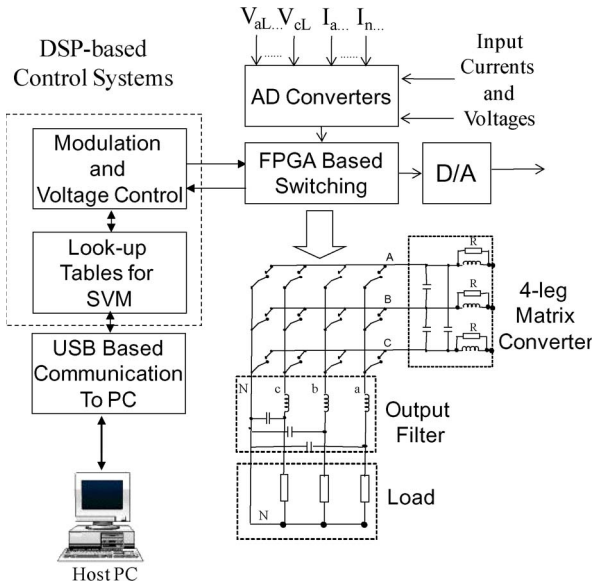

Fig. 12. Experimental system used in this work.

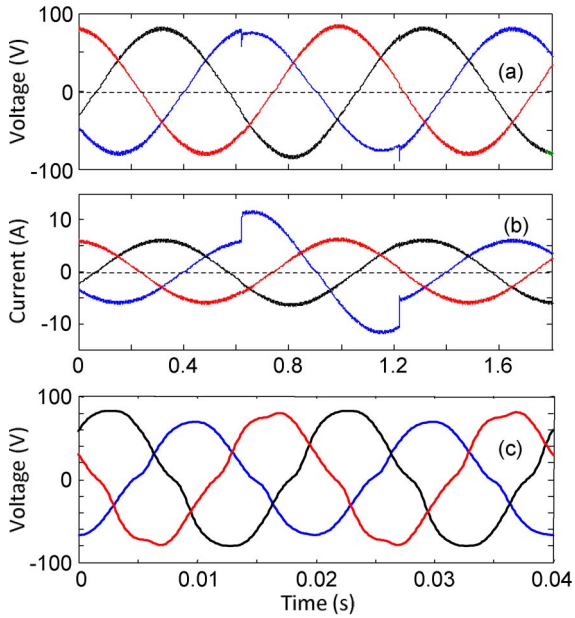

Fig. 13. Response of the d–q control system to an unbalanced load step. (a) Load voltage for 1-Hz operation. (b) Matrix converter output current for 1-Hz operation. (c) Load voltage for 50-Hz operation.

To test the performance of a d–q control system with a low L_f impedance, the output frequency is reduced to 1 Hz. A 5 mH inductance operating at 1 Hz has the equivalent impedance of a 100 μH inductance operating at 50 Hz. For this test the control system has been designed for a bandwidth of about 60 Hz, with a damping coefficient of $\zeta \approx 0.707$. Initially a load of 12 Ω is connected to each phase. In $t \approx 0.5$ s the load in phase a is varied to 6.7 Ω. Fig. 13 shows the response of the system to the unbalanced load step. The load voltages are shown in Fig. 13(a). Notice that the voltage drop in phase a is small (about 4%) which is considered good, for the relatively large load step applied to that phase. Fig. 13(c) shows the steady state performance of the d–q controller when the system is feeding at 50 Hz the unbalanced load corresponding

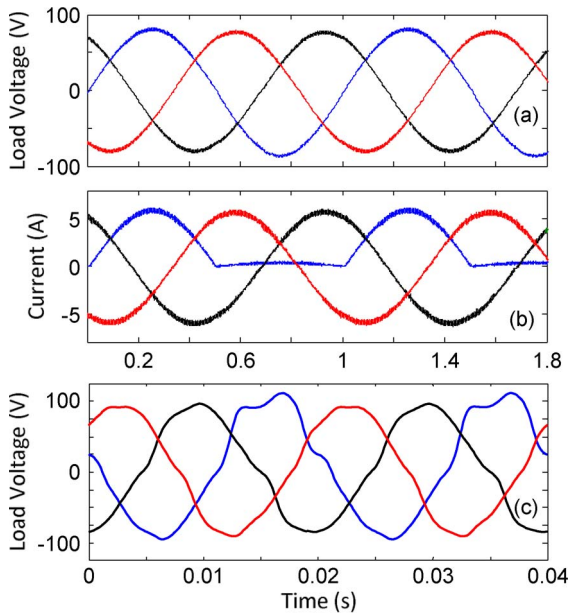

Fig. 14. Control system performance considering a nonlinear load connected in phase a. (a) Load voltages at 1-Hz operation. (b) MC output currents at 1-Hz operation. (c) Load voltages at 50-Hz operation.

to the test in Fig. 13(b). In this case the voltage drop in the L_f impedance cannot be considered negligible and the output voltage is unbalanced and distorted.

Fig. 14 shows the operation of the d–q control system considering a combination of linear load (in two phases) and nonlinear load (in one phase). The latter is implemented using a rectifier diode in series with a resistor.

Fig. 14(a), shows the load voltages. The waveforms have little distortion with good regulation. Fig. 14(b) shows the MC output current. Notice that the current in phase a is highly distorted. In spite of this distortion, the control system has a good performance for this application.

Fig. 14(c) shows the experimental results obtained with an output frequency of 50 Hz and the nonlinear load connected to one phase. Because of the relatively large impedance represented by the output filter inductance at 50 Hz, the waveform in Fig. 14(c) is severely distorted especially in the phase where the nonlinear load is connected.

When the system is operating with a standard d–q controller and considering a relatively large L_f impedance, the controller cannot eliminate the negative and zero-sequence components produced by the unbalanced nonlinear load. This is shown in Fig. 15 for the test corresponding to Fig. 14(c). In this case relatively high zero-sequence voltage (with a peak voltage of about 12 V) is shown in Fig. 15. The negative sequence component, with a peak value below 4 V is also shown in Fig. 15.

V. Experimental Results Obtained With Resonant Controllers

As mentioned before, standard d–q controllers can be applied to systems based in four-leg MCs, operating with some restrictions. Otherwise RCs have a better performance in term of load voltage regulation. Therefore, in this section experimental results obtained with resonant controllers are extensively discussed.

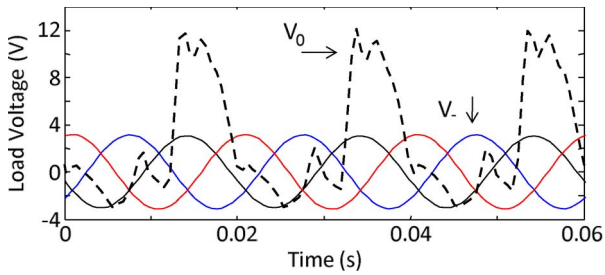

Fig. 15. Zero and negative sequence in the load voltage corresponding to the test in Fig. 14.

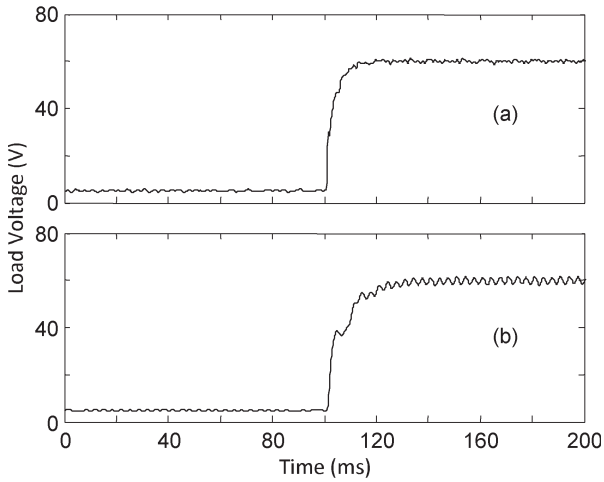

Fig. 16. Control system response for a step in the demanded load voltage. (a) d–q control system. (b) Resonant controller implemented from (18).

A. Design of a RC Using (18)

In this section, a controller implemented using (18) is experimentally tested. A fast d–q controller is designed using root locus for a bandwidth of ≈90 Hz, damping coefficient of ≈0.707. Considering a sampling period of $T_s = 100$ μs, the z-transfer function for this PI controller + lead lag network is

$$G_c(z) = 2\frac{(z-0.8046)}{(z-1)}\frac{(z^2-1.343z+0.4521)}{(z^2-z+0.7466)} \qquad (23)$$

Using (23) and (18) a resonant controller has been implemented for an output frequency of 50 Hz. The d–q controller of (23) and the corresponding RC obtained from (18) were tested in the experimental system of Fig. 12. The decoupling terms of (11) are considered in the d–q implementation, but eliminated from the RC.

In Fig. 16 the control system responses are shown. For the d–q controller of (23), the settling time is about 9 ms, less than half a cycle [see Fig. 16(a)]. For the RC the settling time is about 16 ms with some small oscillations in steady state. The instantaneous load voltages in phase a corresponding to both controllers are shown in Fig. 17. From the first half cycle of the responses, it is concluded that the d–q controller is faster than the "equivalent" resonant controller obtained from (18).

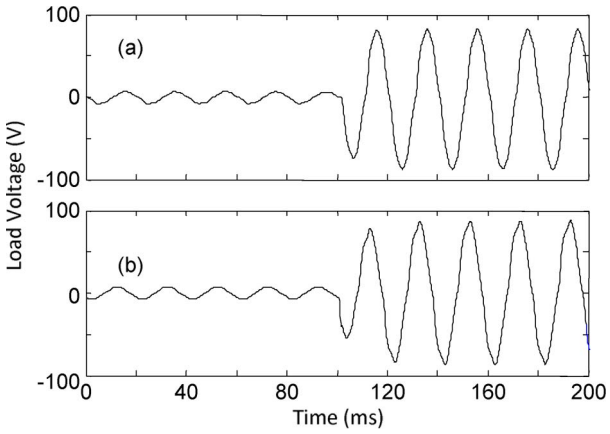

Fig. 17. Instantaneous phase to neutral voltage corresponding to the test in Fig. 16. (a) d–q control system. (b) Resonant controller implemented from (18).

The experimental results shown in Figs. 16 and 17 demonstrate the analysis of Section II. When an a–b–c resonant controller is derived from a controller implemented in a synchronous rotating frame, its dynamic response is not completely equivalent to that of the d–q controller, and part of the bandwidth is lost using (18) (see Fig. 8). Reshaping of the frequency response obtained from (18) is possible using the Bode diagrams.

B. Output Frequency Variation

When output frequency variation is required, for instance in droop control applications, a relatively simple discrete implementation is achieved with d–q controllers. In this case, the angle used to modulate/demodulate the load voltage (see Fig. 2) is obtained as

$$\theta_k = \theta_{k-1} + \omega_o T_s \tag{24}$$

where θ_{k-1} is the value of the angle in the previous sampling period. The output frequency can be adjusted on-line by changing ω_o in (24).

Frequency variations with resonant controllers are more difficult to realize. If it is assumed that the resonant controller has a couple of complex conjugated poles and zeros located in the position shown in Fig. 9, then a variable frequency resonant controller could be achieved using

$$G_c(z) = \frac{(z - re^{j\omega_o T_s})(z - re^{-j\omega_o T_s})}{(z - e^{j\omega_o T_s})(z - e^{-j\omega_o T_s})} = \frac{\left(z^2 - 2r\cos(\omega_o T_s) + r^2\right)}{\left(z^2 - 2\cos(\omega_o T_s) + 1\right)} \tag{25}$$

where "r" is the distance between the complex conjugate zeros and the origin of the z-plane (see Fig. 9). In this paper, good experimental results are obtained using $r = 0.96$. In addition to (25), a lead-lag network has to be considered in the controller implementation [see (20)].

Fig. 18 shows the response of the system when output frequency variation is experimentally implemented considering on-line changes of ω_o in (25). The waveforms obtained with this

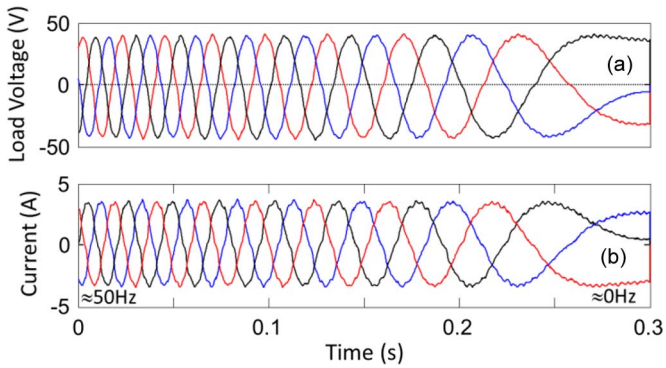

Fig. 18. Frequency variation from 50 Hz to 0 Hz using a resonant controller. (a) Load voltages. (b) MC output current.

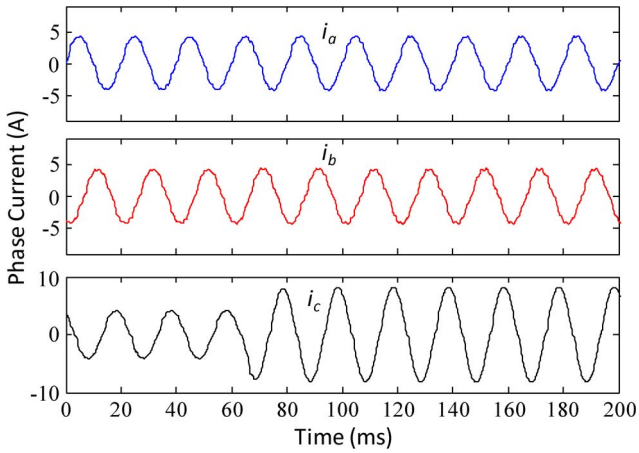

Fig. 19. Four-leg MC output currents for a load step in phase c.

test are appropriate, with little distortion in the load voltages [see Fig. 18(a)] and currents [see Fig. 18(b)]. This is a good dynamic response considering the relatively fast variation in the output frequency (from 50 Hz to 0 Hz).

The resonant controller of (25) has also been experimentally implemented considering a frequency variation from 50 to 100 Hz with good dynamic performance.

C. Performance of an RC Considering Unbalanced Operation

The response of the RC depicted in (20) for an unbalanced load step is shown in Figs. 19 and 20. Before the step all the phases have a resistive load of about 20 Ω. At $t \approx 65$ ms, an additional load is connected in parallel to phase c, reducing the resistance in that phase to 10 ω. In Fig. 19 the 50-Hz four-leg MC output currents are shown. The steady state voltages corresponding to the unbalanced load operation are depicted in Fig. 20. Little distortion is present in the waveforms shown in Figs. 19 and 20.

D. Control System Performance for Nonlinear Load Operation

In this section the performance of the proposed RC controllers is studied considering a nonlinear load connected to one phase. This load is similar to that discussed in Section IV. The THD obtained with two RC topologies is shown in Table I.

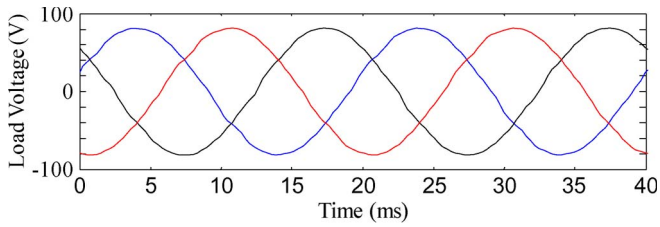

Fig. 20. Load voltages corresponding to the test in Fig. 19.

TABLE I
THD VALUES OBTAINED FOR A NONLINEAR LOAD CONNECTED TO A SINGLE PHASE

Control system	THD
Open loop system	14.7%
Resonant controller I	9.81%
Resonant Controller II	3%

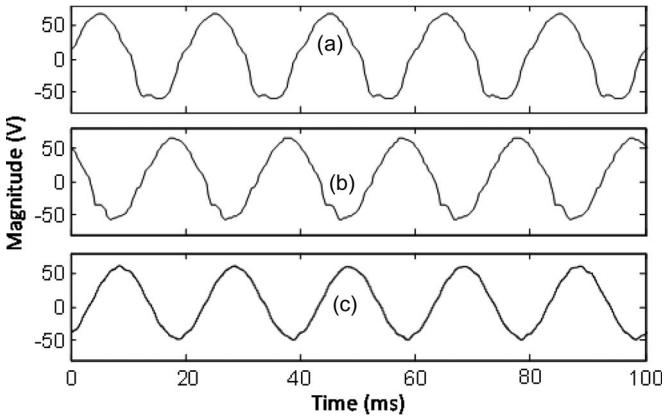

Fig. 21. Performance of the control systems for a nonlinear load connected to one phase. (a) Open loop response. (b) Performance of RC I. (c) Response of the 13th-order resonant controller.

The controller labeled "Resonant Controller I" has a transfer function similar to (20).

The "Resonant Controller II" is an 13th-order controller and is implemented with a transfer function similar to (22). This high-order RC has the best performance in terms of voltage distortion reduction. For open loop operation the THD is about 14.7%

Fig. 21 shows the steady state response for the RCs discussed previously. In Fig. 21(a) open loop operation is shown. Notice the high distortion of the waveform. Fig. 21(b) shows the performance of a single gain RC tuned for 50 Hz. Finally, Fig. 21(c) shows the time response of the high-order RC. The performance of this controller is good, considering the high distortion introduced by the nonlinear load in phase c. A lower THD can be obtained by increasing the controller order to eliminate, for instance, the 7th harmonic. Nevertheless, a tradeoff between THD and computing burden has to be considered to avoid increasing too much the size of the input and output filters by maintaining an acceptable switching frequency.

The zero and negative sequence load voltage corresponding to the test in Fig. 21(c) are shown in Fig. 22. If these experimental results are compared with those shown in Fig. 15, it is concluded that the high-order controller is able to eliminate

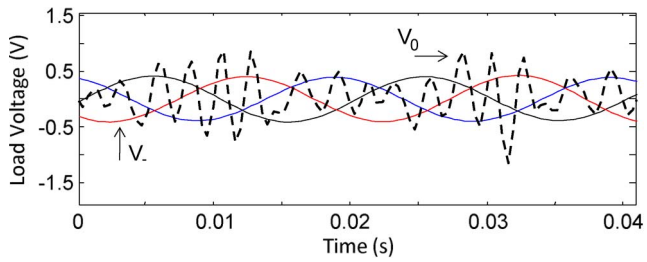

Fig. 22. Zero and negative sequence in the load voltage corresponding to the test in Fig. 21(c).

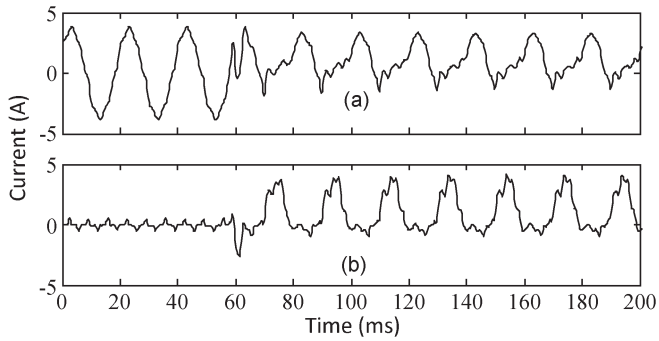

Fig. 23. Phase and neutral current for a nonlinear load step. (a) Current in the phase c of the four-leg MC, where a nonlinear load is connected in $t = 60$ ms. (b) Current in the fouth leg used as load neutral connection.

most of the imbalance and distortion from the load voltage waveforms.

In Fig. 23 the matrix converter output currents for a nonlinear load step change are shown. The load voltages are regulated using the high-order RC of (22). For $t < 60$ ms a linear load of about 10 Ω is connected to phase c. At $t \approx 60$ ms, the linear load is off and a nonlinear load composed of a rectifier diode and a resistance of 10 Ω is connected to this phase. As shown in Fig. 23(a), for $t > 60$ ms the phase current becomes very distorted. Because of the imbalance produced by the nonlinear load, there are zero-sequence components in the neutral current [see Fig. 23(b)].

E. Additional Applications

The SVM algorithm discussed in [12] can be used to synthesise independent line to neutral output voltages. Therefore, some applications, for instance to supply different frequencies to two phases of the 3Φ load, can be implemented using a four-leg MC. This is rather unrealistic, however the results depicted in Figs. 24 and 25 show the flexibility of RCs designed to independently regulate the output voltages of four-leg MCs, modulating even signals of different frequencies at the MC output.

In Fig. 24, the load voltages are shown (peak voltage $\approx$70 V). Two resonant controllers are used in this application. The first controller is tuned to regulate a 50-Hz load voltage in two of the phases. The second controller is designed to regulate a 30-Hz load voltage in the remaining phase.

In Fig. 25 the four-leg MC output currents are shown. Fig. 25(a) shows the 30-Hz current and Fig. 25(b) shows the 50-Hz current Finally, Fig. 25(c) shows the neutral current.

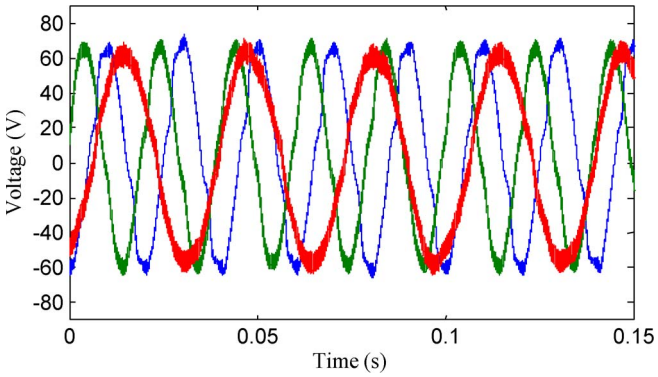

Fig. 24. Performance of a resonant control system regulating load voltages of 50 Hz and 30 Hz.

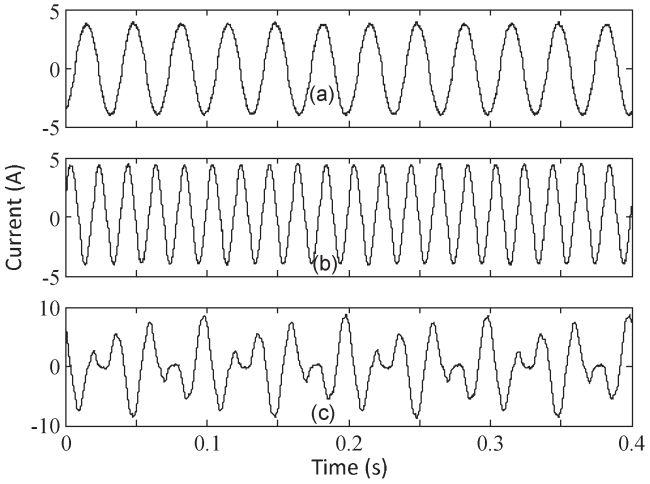

Fig. 25. Currents corresponding to the test in Fig. 24. (a) 30-Hz current. (b) 50-Hz current. (c) Neutral current.

Notice the distortion produced in this current which has strong components of 30- and 50-Hz frequencies.

The performance of RCs has also been tested considering MC outputs with voltages in phase (i.e., without a phase shift of 120° between them). The performance obtained with this test was also considered good.

VI. Conclusion

In this paper, controllers suitable for regulating the phase to neutral voltages of a load fed by a four-leg matrix converter have been tested. The performance of resonant controllers implemented in a–b–c coordinates has been tested to regulate the voltages of nonlinear loads fed by a four-leg MC. Resonant controllers have also been tested considering heavily unbalanced loads. In all the cases the performance has been considered appropriate.

RCs can be derived from d–q controllers designed to operate in synchronous rotating frames. However, the dynamic performance of RCs implemented using (18) is not identical to the corresponding d–q controller unless cross-coupling terms between α–β coordinates [see (9)–(11)] are considered. However, this is not adequate for systems based in four-leg MC, where each phase to neutral voltage could be independently regulated by resonant controllers implemented in a, b, c coordinates.

Another alternative to design RCs is to used standard control design tools such as root-locus, Bode plots, etc. In this case some practical effects, for instance the delay of serial A/D converters, some effects introduced by the digital implementation of the modulation algorithm, etc., can be easily considered.

In this paper,d–q controllers have also been considered for the regulation of the load voltage connected at the output of the four-leg MC. The main disadvantages are in the restricted operating conditions where d–q controllers are applicable. In this paper, it has been shown that these controllers can operate with good dynamic performance in balanced/ slightly unbalanced systems or when the impedance of the MC output filter inductance is small. Otherwise d–q controllers cannot successfully eliminate the negative and zero-sequence components from the load voltages. On the other hand RCs can be used with heavily unbalanced loads and relatively large filter inductances.

Another advantage of RCs is the possibility of eliminating most of the harmonic distortion from the load voltage. However, a tradeoff between processing time and harmonic distortion has to be considered when a high-order controller is implemented.

Appendix
Parameters of the Experimental Rig

Matrix Converter: Input filter $Lf = 0.625$ mH, $Cf = 2$ μF, (delta connected capacitors), four-step commutation method implemented with a 0.7 μs for each step. The matrix converter is controlled with a 10 kHz switching frequency.

MC Output Filter: Output filter implemented with 5 mH inductances and 40 uF capacitors.

Output Load: The filter capacitors are connected in parallel with a resistive load. In the experimental test, the load is implemented using switchable resistor banks of 140 Ω per phase.

References

[1] P. W. Wheeler, J. Rodriguez, J. C. Clare, L. Empringham, and A. Weinstein, "Matrix converters: A technology review," *IEEE Trans. Ind. Electron.*, vol. 49, no. 2, pp. 276–288, Apr. 2002.

[2] M. Aten, G. Towers, C. Whitley, P. Wheeler, J. Clare, and K. Bradley, "Reliability comparison of matrix and other converter topologies," *IEEE Trans. Aerosp. Electron. Syst.*, vol. 42, no. 3, pp. 867–875, Jul. 2006.

[3] T. F. Podlesak, D. C. Katsis, P. W. Wheeler, J. C. Clare, L. Empringham, and M. Bland, "A 150-kVA vector-controlled matrix converter induction motor drive," *IEEE Trans. Ind. Appl.*, vol. 41, no. 3, pp. 841–847, May/Jun. 2005.

[4] P. W. Wheeler, J. C. Clare, L. Empringham, M. Bland, and K. G. Kerris, "Matrix converters," *IEEE Ind. Appl. Mag.*, vol. 10, no. 1, pp. 59–65, Jan./Feb. 2004.

[5] P. W. Wheeler, P. Zanchetta, J. C. Clare, L. Empringham, M. Bland, and D. Katsis, "A utility power supply based on a four-output leg matrix converter," *IEEE Trans. Ind. Appl.*, vol. 44, no. 1, pp. 174–186, Jan./Feb. 2008.

[6] S. L. Arevalo, P. Zanchetta, P. W. Wheeler, A. Trentin, and L. Empringham, "Control and implementation of a matrix-converter-based ac ground power-supply unit for aircraft servicing," *IEEE Trans. Ind. Electron.*, vol. 57, no. 6, pp. 2076–2084, Jun. 2010.

[7] P. Zanchetta, P. W. Wheeler, J. C. Clare, M. Bland, L. Empringham, and D. Katsis, "Control design of a three-phase matrix-converter-based ac–ac mobile utility power supply," *IEEE Trans. Ind. Electron.*, vol. 55, no. 1, pp. 209–217, Jan. 2008.

[8] M. Y. Lee, P. Wheeler, and C. Klumpner, "Space-vector modulated multilevel matrix converter," *IEEE Trans. Ind. Electron.*, vol. 57, no. 10, pp. 3385–3394, Oct. 2010.

[9] R. Cardenas-Dobson, R. Pena, P. Wheeler, and J. Clare, "Experimental validation of a space vector modulation algorithm for four-leg matrix converters," *IEEE Trans. Ind. Electron.*, vol. 58, no. 4, pp. 1282–1293, Apr. 2011.
[10] R. Cardenas, R. Pena, G. Tobar, J. Clare, P. Wheeler, and G. Asher, "Stability analysis of a wind energy conversion system based on a doubly fed induction generator fed by a matrix converter," *IEEE Trans. Ind. Electron.*, vol. 56, no. 10, pp. 4194–4206, Oct. 2009.
[11] D. Casadei, J. Clare, L. Empringham, G. Serra, A. Tani, A. Trentin, P. Wheeler, and L. Zarri, "Large-signal model for the stability analysis of matrix converters," *IEEE Trans. Ind. Electron.*, vol. 54, no. 2, pp. 939–950, Apr. 2007.
[12] R. Cardenas, R. Pena, P. Wheeler, and J. Clare, "Experimental validation of a space vector modulation method for a 4-leg matrix converter," in *Proc. 5th IET Int. Conf. PEMD*, 2010, pp. 1–6.
[13] R. Cardenas, R. Pena, P. Wheeler, and J. Clare, "Resonant controllers for 4-leg matrix converters," in *Proc. IEEE Int. Symp. Ind. Electron.*, 2010, pp. 1027–1032.
[14] N. J. Mason, P. W. Wheeler, and J. C. Clare, "Space vector modulation for a 4-leg matrix converter," in *Proc. IEEE 36th Power Electron. Spec. Conf.*, 2005, pp. 31–38.
[15] K. Borisov and H. L. Ginn, "Multifunctional VSC based on a novel fortescue reference signal generator," *IEEE Trans. Ind. Electron.*, vol. 57, no. 3, pp. 1002–1007, Mar. 2010.
[16] C. Wang and Y. Li, "Analysis and calculation of zero-sequence voltage considering neutral-point potential balancing in three-level NPC converters," *IEEE Trans. Ind. Electron.*, vol. 57, no. 7, pp. 2262–2271, Jul. 2010.
[17] C. L. Fortescue, "Method of symmetrical coordinates applied to the solution of polyphase networks," *AIEE Trans.*, vol. 37, no. 2, pp. 1027–1140, Jul. 1918.
[18] K. Prabha, *Power System Stability and Control*. New York: McGraw-Hill, 1994.
[19] M. Liserre, R. Teodorescu, and F. Blaabjerg, "Multiple harmonics control for three-phase grid converter systems with the use of PI-RES current controller in a rotating frame," *IEEE Trans. Power Electron.*, vol. 21, no. 3, pp. 836–841, May 2006.
[20] C. Lascu, L. Asiminoaei, I. Boldea, and F. Blaabjerg, "Frequency response analysis of current controllers for selective harmonic compensation in active power filters," *IEEE Trans. Ind. Electron.*, vol. 56, no. 2, pp. 337–347, Feb. 2009.
[21] D. N. Zmood, D. G. Holmes, and G. H. Bode, "Frequency-domain analysis of three-phase linear current regulators," *IEEE Trans. Ind. Appl.*, vol. 37, no. 2, pp. 601–610, Mar./Apr. 2001.
[22] D. N. Zmood and D. G. Holmes, "Stationary frame current regulation of PWM inverters with zero steady-state error," *IEEE Trans. Power Electron.*, vol. 18, no. 3, pp. 814–822, May 2003.
[23] A. Timbus, M. Liserre, R. Teodorescu, P. Rodriguez, and F. Blaabjerg, "Evaluation of current controllers for distributed power generation systems," *IEEE Trans. Power Electron.*, vol. 24, no. 3, pp. 654–664, Mar. 2009.
[24] B. Buso and P. Mattavelli, *Digital Control in Power Electronics*, J. Hudgins, Ed. San Rafael, CA: Morgan and Claypool, 2006.
[25] J. G. Hwang, P. W. Lehn, and M. Winkelnkemper, "A generalized class of stationary frame-current controllers for grid-connected ac–dc converters," *IEEE Trans. Power Del.*, vol. 25, no. 4, pp. 2742–2751, Oct. 2010.
[26] C. Sao and P. W. Lehn, "A block diagram approach to reference frame transformation of converter dynamic models," in *Proc. CCECE*, 2006, pp. 2270–2274.
[27] R. Cardenas, R. Pena, P. Wheeler, J. Clare, and G. Asher, "Control of the reactive power supplied by a WECS based on an induction generator fed by a matrix converter," *IEEE Trans. Ind. Electron.*, vol. 56, no. 2, pp. 429–438, Feb. 2009.
[28] R. Pena, R. Cardenas, J. Proboste, J. Clare, and G. Asher, "Wind-diesel generation using doubly fed induction machines," *IEEE Trans. Energy Convers.*, vol. 23, no. 1, pp. 202–214, Mar. 2008.
[29] S. Zhang, K.-J. Tseng, D. M. Vilathgamuwa, T. D. Nguyen, and X.-Y. Wang, "Design of a robust grid interface system for PMSG-based wind turbine generators," *IEEE Trans. Ind. Electron.*, vol. 58, no. 1, pp. 316–328, Jan. 2011.
[30] D. N. Zmood and D. G. Holmes, "Improved voltage regulation for current-source inverters," *IEEE Trans. Ind. Appl.*, vol. 37, no. 4, pp. 1028–1036, Jul./Aug. 2001.
[31] R. Pena, R. Cardenas, E. Reyes, J. Clare, and P. Wheeler, "A topology for multiple generation system with doubly fed induction machines and indirect matrix converter," *IEEE Trans. Ind. Electron.*, vol. 56, no. 10, pp. 4181–4193, Oct. 2009.
[32] R. Pena, R. Cardenas, E. Escobar, J. Clare, and P. Wheeler, "Control system for unbalanced operation of stand-alone doubly fed induction generator," *IEEE Trans. Energy Convers.*, vol. 22, no. 2, pp. 544–545, Jun. 2007.
[33] R. Teodorescu, F. Blaabjerg, M. Liserre, and P. C. Loh, "Proportional-resonant controllers and filters for grid-connected voltage-source converters," *Proc. Inst. Elect. Eng.—Elect. Power Appl.*, vol. 153, no. 5, pp. 750–762, Sep. 2006.
[34] J. W. G. Hwang, M. Winkelnkemper, and P. W. Lehn, "Design of an optimal stationary frame controller for grid connected ac–dc converters," in *Proc. 32nd IEEE IECON*, 2006, pp. 167–172.
[35] A. G. Yepes, F. D. Freijedo, J. Doval-Gandoy, O. López, J. Malvar, and P. Fernandez-Comesaña, "Effects of discretization methods on the performance of resonant controllers," *IEEE Trans. Power Electron.*, vol. 25, no. 7, pp. 1692–1712, Jul. 2010.
[36] L. Harnefors, "Implementation of resonant controllers and filters in fixed-point arithmetic," *IEEE Trans. Ind. Electron.*, vol. 56, no. 4, pp. 1273–1281, Apr. 2009.
[37] G. F. Franklin, J. D. Powell, and M. L. Workman, *Digital Control of Dynamic Systems*. Englewood Cliffs, NJ: Prentice-Hall, 1997.

Roberto Cárdenas (S'95–M'97–SM'07) was born in Punta Arenas, Chile. He received the B.S. degree from the University of Magallanes, Punta Arenas, in 1988, and the M.Sc. and Ph.D degrees from the University of Nottingham, Nottingham, U.K., in 1992 and 1996, respectively.

From 1989 to 1991 and 1996 to 2008, he was a Lecturer in the University of Magallanes. From 1991 to 1996, he was with the Power Electronics Machines and Control Group (PEMC group), University of Nottingham. He is currently an Associate Professor in Power Electronics and Drives with the Electrical Engineering Department, University of Chile, Santiago, Chile. His main interests include control of electrical machines, variable speed drives, and renewable energy systems.

Dr. Cárdenas received the Best Paper Award from the IEEE TRANSACTIONS ON INDUSTRIAL ELECTRONICS in 2004, and the "Ramon Salas Edward" Award for research excellence from the Chilean Institute of Engineers in 2009.

Carlos Juri (S'10) was born in Santiago, Chile, in 1984. He received the B.Eng. degree in electrical engineering from the University of Chile, Santiago, in 2010.

He is currently as a Research Assistant in the Electrical Engineering Department University of Chile. His main interests include renewable generation systems, distributed generation, and power electronics converters.

Rubén Peña (S'95–M'97) was born in Coronel, Chile. He received the Electrical Engineering degree from the University of Concepcion, Concepcion, Chile, in 1984, and the M.Sc. and Ph.D. degrees from the University of Nottingham, Nottingham, U.K., in 1992 and 1996, respectively.

From 1985 to 2008, he was a Lecturer in the University of Magallanes, Punta Arenas. He is currently with the Electrical Engineering Department, University of Concepción, Chile. His main interests are in control of power electronics converters, A.C. drives, and renewable energy systems.

Jon Clare (M'90–SM'04) was born in Bristol, England. He received the B.Sc. and Ph.D. degrees in electrical engineering from The University of Bristol, Bristol, U.K..

From 1984 to 1990, he worked as a Research Assistant and Lecturer at The University of Bristol involved in teaching and research in power electronic systems. Since 1990, he has been with the Power Electronics, Machines and Control Group at the University of Nottingham, Nottingham, U.K. and is currently Professor in Power Electronics. His research interests are in power electronic converters and modulation strategies, variable speed drive systems, and electromagnetic compatibility.

Dr. Clare is a member of the Institution of Engineering Technology.

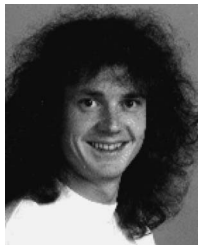

Patrick Wheeler (M'00) received the B.Eng. degree in electrical engineering, in 1990, and the Ph.D. degree for work on Matrix Converters at the University of Bristol, Bristol, U.K., in 1994.

In 1993, he moved to the University of Nottingham, Nottingham, U.K., and worked as a Research Assistant in the Department of Electrical and Electronic Engineering. In 1996, he was appointed Lecturer (subsequently Senior Lecturer in 2002 and Professor in Power Electronic Systems in 2007) with the Power Electronics, Machines and Control Group at the University of Nottingham. His research interests are in variable speed ac Motor Drives, particularly different circuit topologies; power converters for power systems and semiconductor switch use.

Dr. Wheeler is a member of the Institution of Engineering Technology.